Mausam, (1979), **30**, 1, 31-38

551.509.313(215-17)

Spectral integration of a hemispheric barotropic model

H. S. BEDI

Meteorological Office, New Delhi

(*Received 1 March 1978*)

ABSTRACT. A barotropic model for the northern hemisphere is integrated by decomposing the basic horizontal field into a low-order wave spectrum. The spectral representation is in terms of surface spherical harmonics which takes into account sphericity of the earth's surface in a natural way. The initial input for the model is the stream function spectrum derived from geopotential spectrum through linear balance wind relationship. Inclusion of appropriate amount of divergence in an empirical way improves the overall performance of the model. The performance of the model in relation to persistence is discussed.

1. Introduction

Any numerical weather prediction model without sufficient resolution in the horizontal and vertical cannot be expected to simulate the behaviour of the atmosphere adequately. Nevertheless, single level barotropic model based on the principle of conservation of absolute vorticity has been found useful in predicting the large-scale behaviour of two-dimensional atmospheric flow. In a non-divergent barotropic model the total kinetic energy and vorticity over the model domain remain conserved, though, through the advective processes, the exchanges of kinetic energy and vorticity among various scales of motion take place freely. In the actual atmosphere these conservative properties are valid more for an extended area (hemisphere or globe), rather than for a limited area. The usual method of integration of atmospheric models is by finite difference approximations. Even though the differential equations of the model may conserve energy and vorticity, the actual integration may not do so unless the finite difference schemes are designed carefully with such a purpose in view. Besides, special care is required to control truncation errors and computational instabilities. During recent years, an alternative approach based on Galerkin (spectral) approximation has shown some attractive advantages. If the original equations are bounded and their exact solution satisfies certain integral constraints; then the spectral approximation is also bounded and conserves required integral constraints. In addition, truncation errors and computational instabilities are controlled. A careful choice of basis functions often yields fast convergence of approximation to the original solution. For the meteorological equations in spherical co-ordinate system, the surface spherical harmonics can be shown to be appropriate basis functions. The present study reports the results of integration of barotropic model over the northern hemisphere by such spectral technique.

2. Input data base

The basic input to the model is the geopotential height data for 500 mb level collected at 5° Lat.-Long. interval over the northern hemisphere. The spectral approach is based on approximation of this data field in terms of a truncated series of surface spherical harmonics. In the absence of data from the southern hemisphere we assume the symmetry of geopotential field across the equator. This assumption is justified, as it ensures the continuity of temperature and zonal wind across the equator. Thus we have the spectral representation of geopotential in terms of surface spherical harmonics symmetric with respect to equator as

$$h(\mu, \lambda, t) = \sum_{m=-M}^{M} \sum_{n=|m|,2}^{|m|+N} \phi_n^m(t).\, Y_n^m(\mu, \lambda) \quad (1)$$

$Y_n^m(\mu, \lambda)$ is surface spherical harmonics and is given by

$$Y_n^m(\mu, \lambda) = P_n^m(\mu)\, e^{im\lambda} \quad (2)$$

Here $P_n^m(\mu)$ is associated Legendre function of first kind of order m and degree n normalised over

the hemisphere and is given by

$$P_n^m(\mu) = \frac{\sqrt{2}}{2^n . n!}\left[\frac{(2n+1)}{2}\cdot\frac{(n-m)!}{(n+m)!}\right]^{\frac{1}{2}} . \\ . (1-\mu^2)^{m/2}\ \frac{d^{n+m}(\mu^2-1)^n}{d\mu^{n+m}} \qquad (3)$$
$$\text{for } n \geqslant m$$
$$= 0 \qquad \text{for } n < m$$

λ is longitude and $\mu = \sin\phi$, where ϕ is latitude. ${\phi_n}^m$ is complex amplitude, a function of time.

The second summation in (1) is at the interval of 2 and the series is truncated at $M = 15$ and $N = 12$, so that in all 112 components with spectral configuration

$0 \leqslant m \leqslant 15$; $n-m = 0, 2, 4 \ldots\ldots\ldots N-12$ were used for expansion.

Large-scale atmospheric flow patterns have been found to be represented to a high degree of accuracy by these limited number of spectral components (Bedi 1976).

The spectral amplitudes of stream function were obtained by the solution of linear balance equation in its spectral form

$$n(n+2)\,{\alpha_n}^m\,{\psi^m}_{n+1} + (n-1)(n+1)\,{\beta_n}^m\,{\psi^m}_{n-1} \\ = \frac{n(n+1)}{2\Omega}\,{\phi_n}^m \qquad (4)$$

with boundary conditions

$${\psi^m}_{m-1} = 0 \qquad \text{for } m \neq 0$$
$${\psi_1}^0 = -\frac{\sqrt{3}}{2}\,M \text{ for } m=0$$

where M is the mean zonal angular momentum and is given by

$$M = \int_0^{\pi/2}\int_0^{2\pi} a\,(u_g \cos\phi)\cos\phi\; d\lambda .\, d\phi \qquad (5)$$

a is the radius of earth and u_g, the geostrophic wind.

${\psi_n}^m$ and ${\phi_n}^m$ in (4) are the amplitudes of stream function and geopotential fields respectively, Ω is the angular velocity of the earth and ${\alpha_n}^m$ and ${\beta_n}^m$ are given by

$${\alpha_n}^m = \left[\frac{(n+1-m)\ (n+1+m)}{(2n+1)\ (2n+3)}\right]^{1/2},$$
$${\beta_n}^m = \left[\frac{(n-m)\ (n+m)}{(2n-1)\ (2n+1)}\right]^{1/2} \qquad (6)$$

The configuration of stream function spectrum derived was $0 \leqslant m \leqslant 15$ $n-m = 1, 3, 5, \ldots\ldots N = 13$

Details of procedure for the analysis of hemispheric geopotential field into spherical harmonic components and the solution of Eqn. (4) are given by Bedi (1976). It is also shown there that the stream function field thus obtained does not permit any cross-equatorial transport of mass or energy, so that, the northern hemisphere becomes a closed domain.

3. Spectral barotropic model

The barotropic vorticity equation governing a two-dimensional non-diverent flow is

$$\nabla^2\,\frac{\partial}{\partial t}\,\psi = -J(\psi, \nabla^2\psi + f) \qquad (7)$$

Eqn. (7) can be shown to conserve total kinetic energy and vorticity over a closed domain. However, the flow patterns predicted by this equation, particularly for an extended area show large systematic errors. Wolff (1958) diagnosed these errors due to the retrogression of ultra-long waves 1, 2 and 3 in the model forecast. In the actual atmosphere these waves are anchored by the topographic and thermal forcings and are therefore quasi-stationary. Wolff also suggested an emperical method of arresting such retrogression as a result of which the forecasts did show improvement. Cressman (1958) investigated this problem further and suggested that the large-scale divergence in the real atmosphere inhibits the retrogression of very long waves. The effect of such divergence can be incorporated emperically and the divergent barotropic model takes the form

$$(\nabla^2 - \delta)\,\frac{\partial}{\partial t}\,\psi = -J(\psi, \nabla^2\psi + f) \qquad (8)$$

where δ was chosen empirically.

The spectral form of (8) is

$$[n(n+1) + \gamma^2]\ \frac{d}{dt}\ {\psi_n}^m \\ = a^2\,{\mathbf{J}_n}^m(\psi, \nabla^2\psi) + 2i\,\Omega\,m\,{\psi_n}^m \qquad (9)$$

where $\gamma^2 = -a^2\delta$ is a non-dimensional constant incorporating divergence effect and ${\mathbf{J}_n}^m(\psi, \nabla^2\psi)$ is spectral transform of $J(\psi, \nabla^2\psi)$. On linearising Eqn. (9), the phase speed C_γ of spherical harmonic wave of degree n is given by

$$C_\gamma = -2\,\Omega/[n(n+1) + \gamma^2] \qquad (10)$$

For $\gamma = 0$ (no divergence), the harmonic waves have maximum speed. For values of γ greater than zero the phase speed decreases depending upon the degree of harmonic and value of γ. The modification in phase speed of spherical harmonic waves of different degrees as given by the ratio C_γ/C_0 for

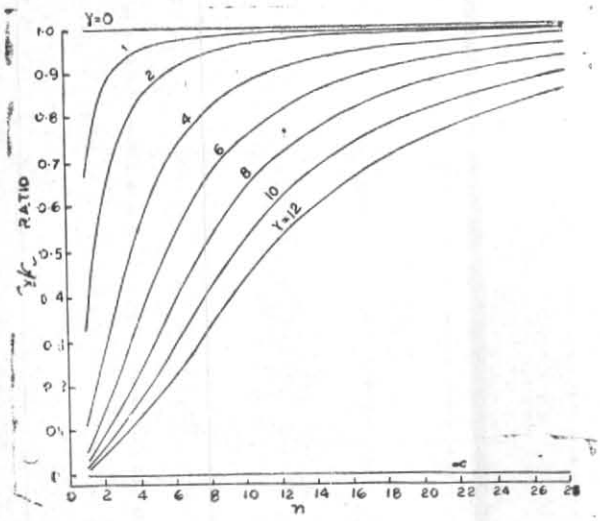

Fig. 1. Effect of divergence on phase speed of waves in linear model

different values of γ is shown in Fig. 1. The inclusion of divergence slows down the movement of all scales of waves; the phase speed of larger waves being modified significantly while that of small waves changes very little.

To study the behaviour of divergent barotropic spectral model, 24-hour forecasts for 10 summer and 10 winter situations were prepared for the northern hemisphere by integrating Eqn. (9). The effect of the magnitude of divergence on these forecasts was specially investigated. In each of these forecasts, the divergence parameter γ was progressively increased from 0 to 12 in the steps of 2.

For calculating the spectral form of non-linear Jacobian term, $J(\psi, \nabla^2\psi)$ the transform method (Orszag 1970, Machenhaur and Rasmussen 1972) was followed. The method consists of following basic steps :

(*i*) Transformation of different components of non-linear terms from spherical harmonic domain to Fourier domain on fixed latitudes.

(*ii*) Transformation of these Fourier components to grid point values in physical space through inverse Fourier transform.

(*iii*) Computation of non-linear term in physical space at each of the grid points from grid point values obtained under step (*ii*).

(*iv*) Transformation of this non-linear field from physical space to Fourier domain on latitude circles.

(*v*) Transformation of these Fourier components on latitude circles to spherical harmonic domain.

The transform method requires frequent application of Fourier and inverse Fourier transforms. Though the Fast Fourier Transform (FFT) technique was not used, the data under analysis were suitably folded and refolded to cut down number of computation steps considerably. For calculation of spherical harmonic components under step (*v*) above, Gaussian quadrature was used. The minimum number of points used on latitude circles for Fourier transform and the latitudes of Gaussian quadrature were so chosen as to ensure the transform process free from aliasing. In the present case for $M = 15$ and $N=13$, 64 points for Fourier transform and 20 Gaussian latitudes were found sufficient. To minimise truncation errors transform computations were done with double precision. The time integration scheme consisted of first forward time step followed by leapfrog steps with two hours time intervals.

4. Effect of divergence correction

Fig. 2 shows the 24 hours forecast movement of different wave components averaged for all the 20 cases studied. The actually observed 24 hours average movement is also shown by dotted line. It is seen that as the value of divergence parameter γ is increased, the movement of waves is arrested. The decrease in the retrogression with the increase of divergence parameter is very large for $n \leqslant 4$. The effect of divergence on the phase speed of waves becomes negligible for $n \geqslant 8$. It is also seen that the forecast movement of spherical harmonic waves with n ranging between 8 and 22 is in very close agreement with their actual movement. However, somewhat faster (by about 2° to 5° Long. day^{-1}) movement is forecast is noticed for harmonics with $n = 22$ to 28. Thus, for a large part of spectrum $\gamma=6$ to 8 seems to be an appropriate divergence parameter for 24 hours forecast. Separate examination of summer and winter forecasts did not show any dependance of divergence parameter on season.

The effects of divergence parameter on the 24 hours forecast kinetic energy and vorticity were also examined. It was noticed that the inclusion of divergence did not strictly conserve these parameters. The difference between initial kinetic energy and vorticity and their 24 hours forecast, on the average, showed an increase with the increase of divergence upto $\gamma=6$ and remained nearly steady thereafter. The differences between their initial and forecast values were, however, small, *i.e.*, less than 1 to 2 per cent of their initial values.

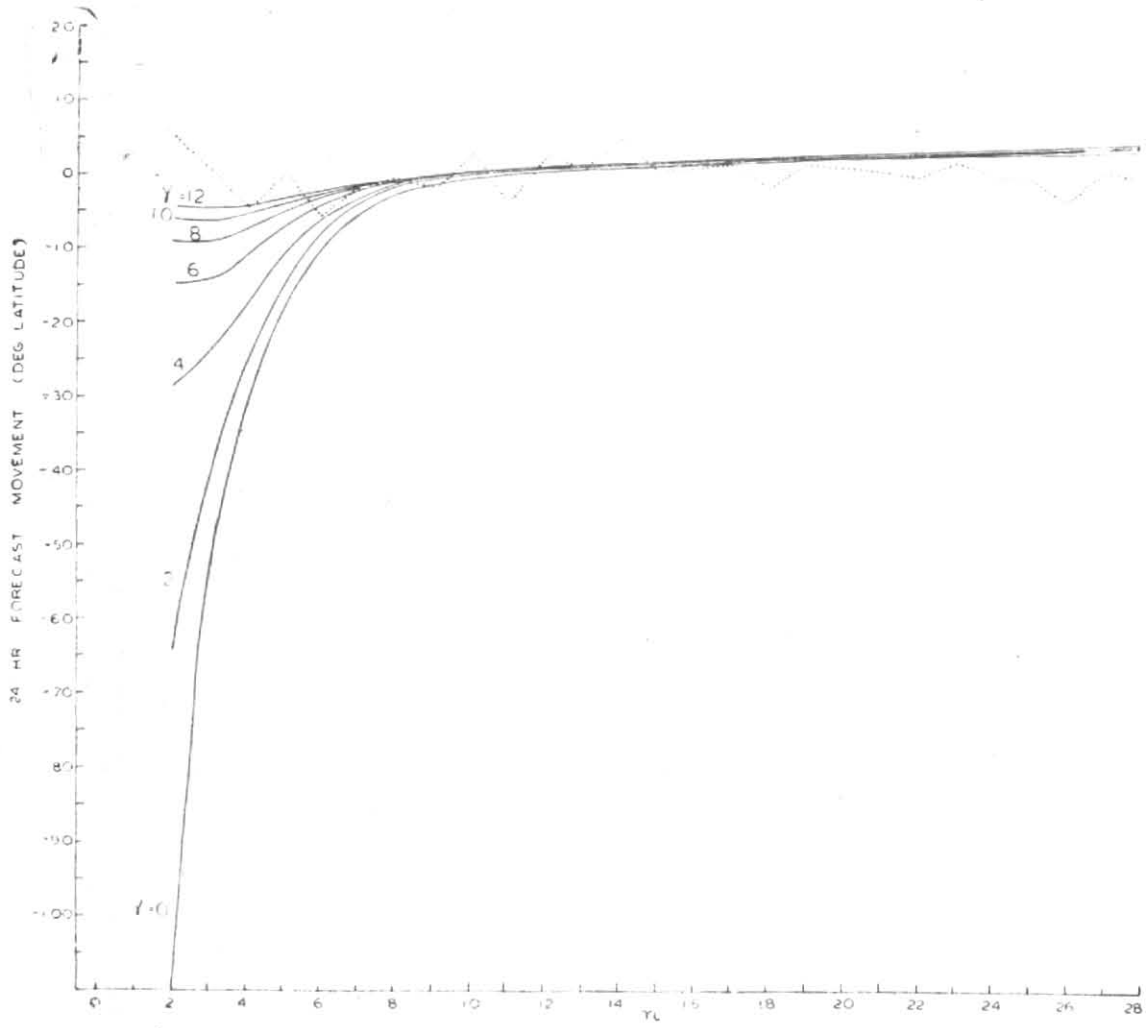

Fig. 2. Effect of divergence on 24-hr forecast movement of spherical harmonic waves. Observed average movement is shown by dotted line

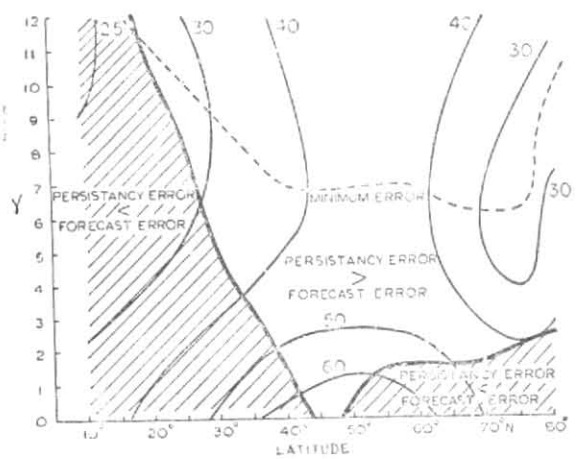

Fig. 3. Variation of root-mean-square error of 24-hr forecast with divergence parameter γ
(Unit : gpm)

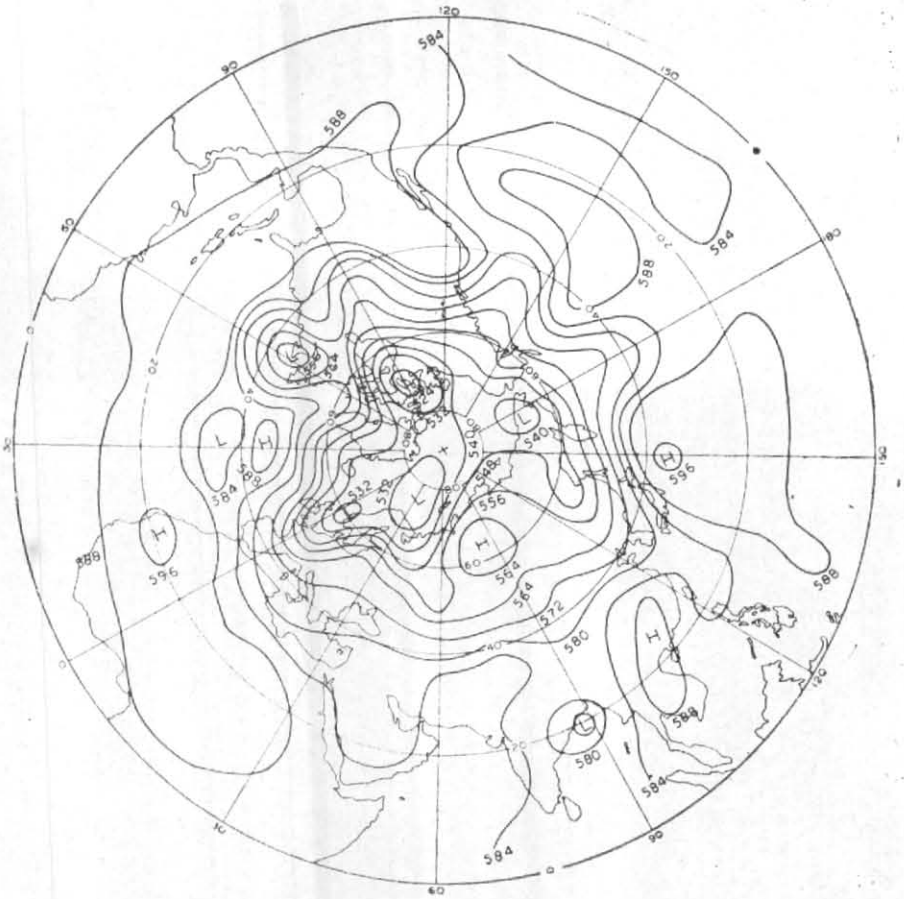

Fig. 4. 500 mb flow patterns at 00 GMT on 10 September 1976

The overall effect of divergence in barotropic model in terms of root-mean-square error of forecast is shown in Fig. 3. Over the shaded area in the figure the root-mean-square error of the model forecast is more than that for the persistence. The accuracy of forecast by non-divergent model ($\gamma=0$) is poorer than that of persistency forecast nearly over all the latitudes. Inclusion of divergence improves the accuracy of forecast at all latitudes. To the north of 30° N, barotropic model with $\gamma>6$ gives better forecast than persistence. Best forecast (lowest RMS error) in the middle and high latitudes is achieved with $\gamma=7$. Over the lower latitudes, to the south of 20° N, the forecast by divergent barotropic model remains inferior to persistency even for $\gamma=10$.

On these considerations, it was decided to take the value of γ as 8 to achieve an overall improvement in 24 hours forecast. Leith (1974) found $\gamma=7$ to be a suitable divergence parameter to give overall best forecast for 48 hours.

5. A case study

Under this section we shall examine the performance of divergent barotropic model in predicting 24 hours and 48 hours 500 mb flow patterns starting from 00 GMT of 10 September 1976 in some details. This particular situation was chosen on the consideration that there were some well defined synoptic systems in the lower as well as in the higher latitudes on this day. The flow patterns based on 112 surface spherical harmonic components for this situation are shown in Fig. 4. In the middle and higher latitudes, the flow exhibits 5 to 6 zonal waves. Over the middle and higher latitudes the most well marked low pressure system lies over the north Atlantic Ocean near the east coast of North America. Another well marked low pressure system lies over north Canada with associated trough extending upto 35° N along about 90° W. Over the lower latitudes a well marked low pressure system lies over the head Bay of Bengal. Also a well marked trough lies over the East China Sea.

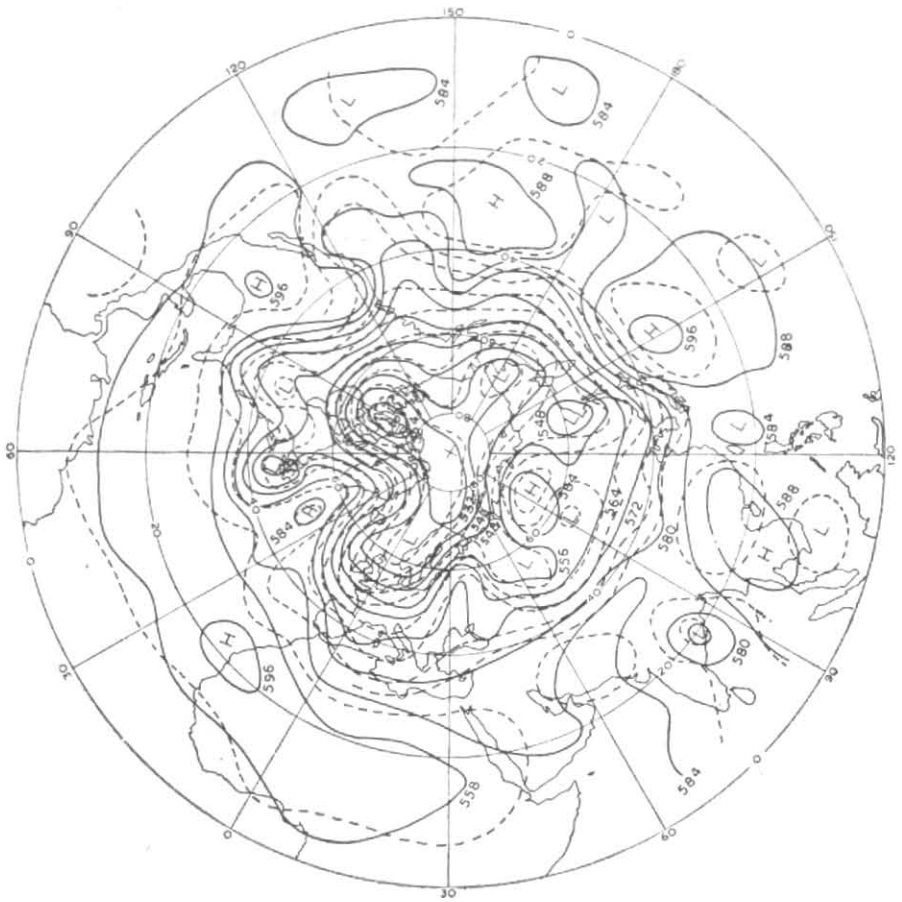

Fig. 5. 24-hr forecast (full lines) and actually observed patterns at 00 GMT on 11 September 1976 (dotted lines)

Fig. 5 shows the 24-hour forecast together with actually realised flow patterns for 00 GMT on 11 September 1976. Over the middle latitudes the forecast flow patterns are in well agreement with the actually observed field. On the average, the 24-hr forecast shows an eastward movement of troughs and ridges by about 5° to 10° longitude which is in well agreement with their actual movement. However, the trough extending from the Norwegian Sea to Spain shows retrogression by about 10° longitude. In actual also, this trough is found to remain stationary or retrograte slightly. Over the lower latitudes, the low pressure system over the head Bay of Bengal is forecasted to move westwards by about 2.5°. This is in agreement with actual movement.

The 48-hr forecast and actually realised fields are shown in Fig.6. As may be expected, as compared to 24-hr forecast, the 48-hr forecast patterns are in less agreement with the actually realised flow. The forecast troughs over the Norwegian Sea, the north Atlantic Ocean and North America are fairly in agreement with the actually observed troughs over these areas. Over north Asia, the forecast and actual systems are not in well agreement. The low pressure area over India shows forecast position near 20°N and 77.5°E, while the actually observed position is about 5 degrees to the east of it.

TABLE 1

Mean RMS error (gpm)

Lat. (°N)	24 hr		48 hr	
	Forecast	Persistence	Forecast	Persistence
0-35	29	30	46	38
35-85	42	70	80	109
0-85	39	57	70	87

The latitudinal variation of the root-mean-square error of model forecast and persistency forecast are shown in Fig. 7. Table 1 gives their mean values for lower and higher latitudes.

It is seen that the behaviour of RMS errors over the regions to the north and south of 35°N is much different. The RMS error of forecasts as well as of persistency is maximum over the latitudinal

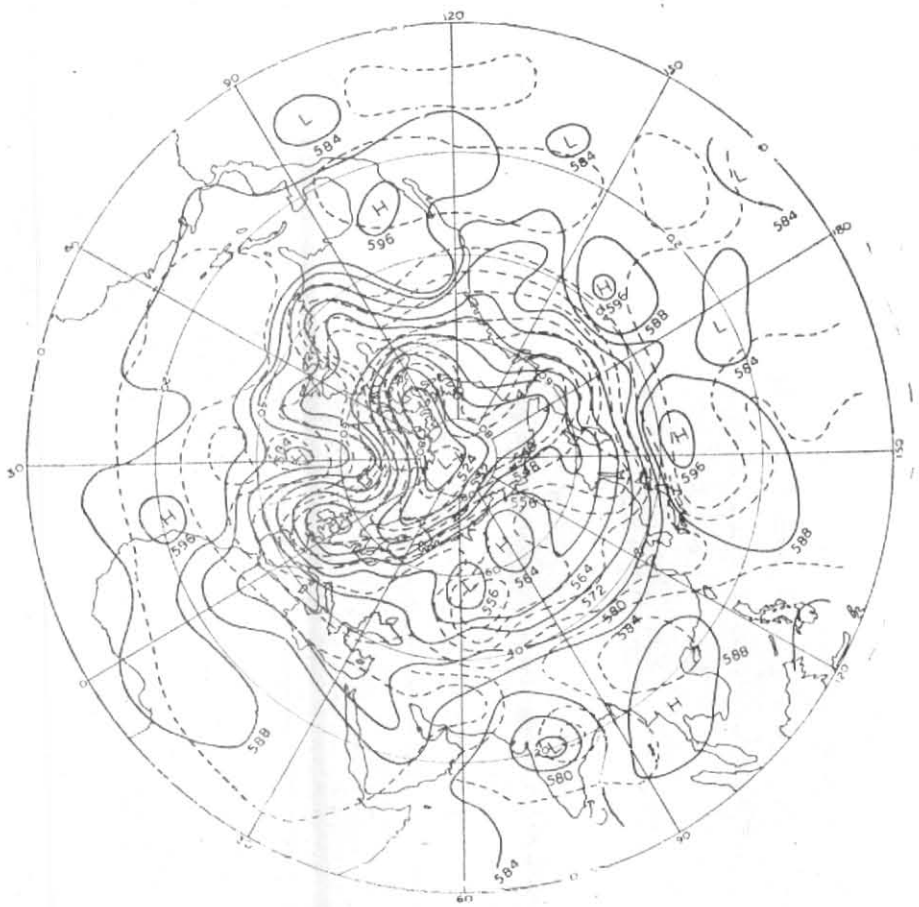

Fig. 6. 48-hr forecast (full lines) and actually observed patterns at 00 GMT on 12 September 1977 (dotted lines)

belt between 45° to 65°N which is dominated by mid-latitude systems. To the north of 35°N, the performance of model is better than persistency up-to 48 hours. To the south of this latitude, the 24 hours forecast and persistence have nearly equal RMS error, while the 48 hours forecast is inferior to persistence. For the whole northern hemisphere, the RMS error for 24 hours as well as 48 hours forecasts is less than that for persistence forecast.

Fig. 8 shows the changes occurring in the kinetic energy and its exchanges during the course of integration. In this particular case, the zonal flow contains about 25 per cent of the total kinetic energy. A slight decrease (about 2 per cent) occurred in zonal kinetic energy during 48 hours integration. This decrease is consistent with the kinetic energy exchanges which show zonal to eddy energy exchanges throughout the course of integration. The eddy kinetic energy as well as total kinetic energy show a very small increase (less than 1 per cent) during 48 hours integration. These energy values show 4 hourly oscillations due to decoupling of solution at alternate time steps, which is characteristic of leapfrog time integration scheme. The amplitude of these oscillations is within about 2 per cent of respective energy values. Such oscillations are noticed in zonal kinetic energy and kinetic energy exchanges also but are not clearly brought out due to less resolution of their variations in the figure.

6. Concluding remarks

From above we may conclude that the barotropic spectral model with the inclusion of suitable amount of large-scale divergence ($\gamma=8$) and a relatively low-order spectral resolution is capable of giving useful 24 and 48-hr forecasts in comparison to persistency in the middle and high latitudes. Over the low latitudes, however, the performance of the model is not much superior to persistency even for 24-hr forecast, though the forecast movement of well marked low pressure system was fairly correct. Besides the inherent limitation of this single layer model, the unsatisfactory performance of the model in the lower latitudes may also be due to :

(*i*) Data sparcity in lower latitudes which effects the accuracy of analysis.

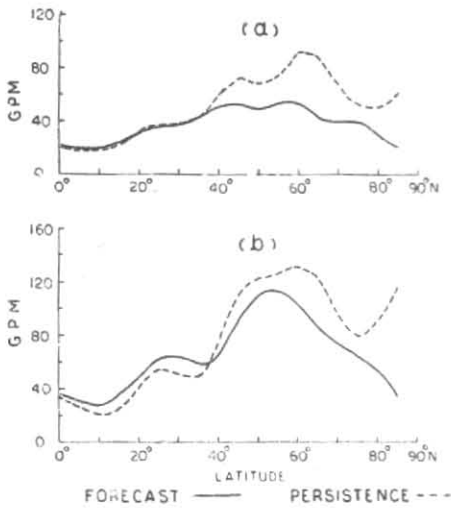

Fig. 7. Latitudinal variation of root-mean-square error of forecast (full line) and persistence (dotted line)

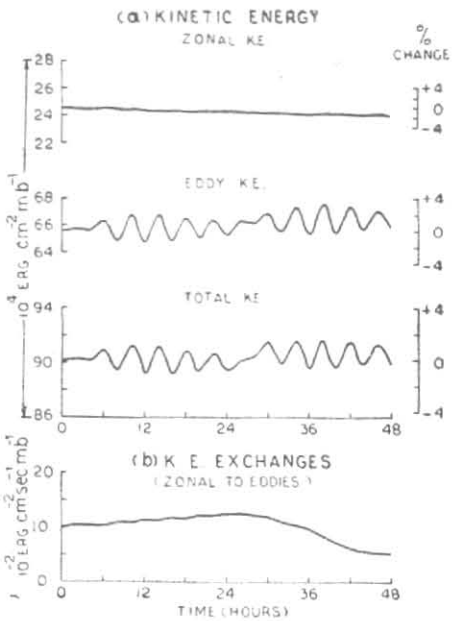

Fig. 8. Variation of kinetic energy and kinetic energy exchanges during integration

(*ii*) The model is restricted to the northern hemisphere and does not provide for any interhemispheric exchanges which may be important for low latitude systems. Possibly, the extension of model over the whole globe may improve its performance over low latitudes.

(*iii*) Relatively small day to day variations of geopotential field over low latitudes account for high persistency over these latitudes against which the forecast performance has been tested.

References

Bedi, H. S., 1976, *Indian J. Met. Hydrol. Geophys.*, **27** : 397-408.

Cressman, G. P., 1958, *Mon. Weath. Rev.*, **88** : 293-297.

Leith, C. E., 1974, Spectral statistical-dynamical forecast experiments. Report on International Symposium on Spectral Methods in NWP. GARP Rep No. 7, Copenhagen, 1974 : 445-455.

Machanhaur, B. and Rasmussen, E., 1972, On the integration of spectral hydrodynamic equations by transform method. Copenhagen University, Institute of Theoretical Meteorology Rep. No. 3, 44 pp.

Orszag, S. A., 1970, *J. atmos. Sci.*, **27** : 890-895.

Wolff, P. M., 1958, *Mon. Weath. Rev.*, **86** : 245-250.